Journal of Nuclear Medicine, published on May 15, 2020 as doi:10.2967/jnumed.120.243113

Radiolabeled cCPE Peptides for SPECT Imaging of Claudin-4 Overexpression in Pancreatic Cancer

Julia Baguña Torres[1], Michael Mosley[1], Sofia Koustoulidou[1], Samantha Hopkins[1], Stefan Knapp[2,3], Apirat Chaikuad[2], Masuo Kondoh[4], Keisuke Tachibana[4], Veerle Kersemans[1] and Bart Cornelissen[1*]

[1] Cancer Research UK and Medical Research Council Oxford Institute for Radiation Oncology, University of Oxford, UK

[2] Institute of Pharmaceutical Chemistry and Structure Genomics Consortium (SGC), Goethe-University Frankfurt, 60438 Frankfurt am Main, Germany

[3] German Cancer Network (DKTK), site Mainz-Frankfurt

[4] Graduate School of Pharmaceutical Sciences, Osaka University, 1-6 Yamadaoka, Suita, Osaka, 565-0871, Japan

Word count: 5,181
Running title: cCPE peptides for imaging claudin-4
Key words: Claudin-4, Pancreatic Ductal Adenocarcinoma, Early Diagnosis, SPECT Imaging

Competing financial interests. The authors have no financial conflicts of interest to declare.

*** To whom correspondence should be addressed:**

Professor Bart Cornelissen, PhD
University of Oxford
CRUK/MRC Oxford Institute for Radiation Oncology, Department of Oncology
Old Road Campus Research Building
Off Roosevelt Drive
Oxford OX3 7LJ, UK
Tel: +44 (0)1865 857126
bart.cornelissen@oncology.ox.ac.uk

ABSTRACT

Introduction: Overexpression of tight junction protein claudin-4 has been detected in primary and metastatic pancreatic cancer tissue, and is associated with better prognosis in patients. Non-invasive measurement of claudin-4 expression by imaging methods could provide a means for accelerating detection and stratifying patients into risk groups. *Clostridium perfringens* enterotoxin (CPE) is a natural ligand for claudin-4 and holds potential as a targeting vector for molecular imaging of claudin-4 overexpression. A glutathione S-transferases (GST)-tagged version of the C-terminus of CPE (cCPE) was previously used to delineate claudin-4 overexpression by single photon emission computed tomography (SPECT), but showed modest binding affinity and slow blood clearance *in vivo*.

Materials and methods: Based on the crystal structure of cCPE, a series of smaller-sized $cCPE_{194-319}$ mutants with putatively improved binding affinity for claudin-4 were generated by site-directed mutagenesis (SDM). All peptides were conjugated site-specifically on a C-terminal cysteine using maleimide- diethylenetriamine pentaacetate (DTPA) to enable radiolabelling with ^{111}In. The binding affinity of all radioconjugates was evaluated in claudin-4-expressing PSN-1 cells and HT1080 negative controls. The specificity of all cCPE mutants to claudin-4 was assessed in HT1080 cells stably transfected with claudin-4. SPECT/ computerised tomography (CT) imaging of BALB/c Nude mice bearing PSN-1 or HT1080 tumour xenografts was performed to determine the claudin-4-targeting ability of these peptides *in vivo*.

Results: Uptake of all cCPE-based radioconjugates was significantly higher in PSN-1 cells compared to HT1080 negative controls. All peptides showed a marked improvement in affinity for claudin-4 *in vitro* when compared to previously reported values (K_D values of 2.2 ± 0.8, 3 ± 0.1, 4.2 ± 0.5 nM, 10 ± 0.9 and 9.7 ± 0.7 nM). Blood clearance of [^{111}In]In-$cCPE_{194-319}$, as measured

by SPECT, was considerably faster when compared to that of [^{111}In]In-cCPE.GST ($t_{1/2}$<1 min). All radiopeptides showed significantly higher accumulation in PSN-1 xenografts than HT1080 tumours at 90 min post-injection of the tracer ([^{111}In]In-cCPE$_{194-319}$: 2.7 ± 0.8 vs 0.4 ± 0.1 %ID/g, P<0.001; [^{111}In]In-S313A: 2.3 ± 0.9 vs 0.5 ± 0.1 %ID/g, P<0.01; [^{111}In]In-S307A+N309A+S313A: 2 ± 0.4 vs 0.3 ± 0.1 %ID/g, P<0.01; [^{111}In]In- D284A: 2 ± 0.2 vs 0.7 ± 0.1 %ID/g, P<0.05; [^{111}In]In- L254F+K257D: 6.3 ± 0.9 vs 0.7 ± 0.2 %ID/g, P<0.001).

Conclusion: These optimised cCPE-based SPECT imaging agents show great promise as claudin-4-targeting vectors for *in vivo* imaging of claudin-4 overexpression in pancreatic cancer.

INTRODUCTION

Pancreatic ductal adenocarcinoma (PDAC) is predicted to become the second-leading cause of cancer-related death within the next decade, with current 5-year survival rates reaching less than 5%. This poor prognosis is partly due to late diagnosis of this mostly non-symptomatic disease at the metastatic stage, and mostly in the emergency medicine setting (*1,2*). Currently, the best probability for long-term survival is surgical resection. However, this is only possible when the disease is still in its early stages and confined to the pancreas.

Radionuclide-based imaging agents for single photon emission computed tomography (SPECT) and positron emission tomography (PET) are exquisitely sensitive tools, capable of detecting molecular markers associated with malignant tissue in vivo. The use of these targeted molecular probes has the potential to greatly improve the diagnosis of pancreatic cancer by enabling the detection of neoplastic transformation and providing functional and prognostic information about the disease. Radiotracers such as the fluorinated glucose analogue 2-[^{18}F]fluoro-2-deoxy-D-glucose ([^{18}F]FDG) have proved able to detect PDAC, distinguish benign mass-forming lesions, and exclude patients with multiple and distant occult metastatic disease from non-beneficial surgery (*3*). However, the use of [^{18}F]FDG-PET as an early diagnostic test is hampered by an inability to distinguish PDAC from chronic/autoimmune pancreatitis (*4,5*), or for treatment evaluation in PDAC during chemo- or radiochemotherapy (*6,7*). Use of other PET imaging agents in pancreatic cancer patients, such as [^{18}F]fluoromisonidazole and [^{18}F]fluoro-3′-deoxy-3′-l-fluorothymidine have produced mixed results, highlighting the need for alternative tools to assess prognosis and treatment response (*8,9*). Targeting more disease-specific molecular markers could therefore considerably aid in the early detection and characterisation of pancreatic cancer lesions.

Claudin transmembrane proteins are considered the structural and functional backbone of tight junction complexes in epithelial and endothelial cells (*10-12*). As tumourigenesis is often accompanied by tight junction disruption and subsequent loss of cell adhesion and polarity, it is not surprising that expression of several claudins is dysregulated in many cancers of epithelial origin. In particular, claudin-4 has been shown to be overexpressed in primary and metastatic pancreatic cancer tissue, including pancreatic intraepithelial neoplasia (PanIN), the most common precursor lesion to PDAC (*13*). Unlike previous biomarkers, increased expression of claudin-4 has not been reported in chronic pancreatitis, which makes this protein an attractive target for early detection of PDAC (*14*). Furthermore, claudin-4 overexpression has been identified as a potent inhibitor of the invasive and metastatic phenotypes of pancreatic cancer cells and correlates with better outcome in PDAC patients (*15,16*). Knockdown studies in ovarian cancer cells suggest that this positive effect of claudin-4 overexpression may be due to its ability to sustain the expression of E-cadherin and limit β-catenin signalling (*17,18*). Hence, claudin-4 can be regarded not only as a promising biomarker for early detection of PDAC but also as a cancer type-specific prognostic indicator.

Clostridium perfringens enterotoxin (CPE, 35 kDa), a natural ligand for claudin-4, has been previously evaluated as a claudin-4-targeting vector for diagnostic and therapeutic purposes. CPE causes the symptoms of type A food poisoning and some non-foodborne gastrointestinal diseases by triggering the lysis of intestinal epithelial cells through its interaction with claudin-4 receptors. Notably, CPE cytotoxicity is mediated by its N-terminus (NH_2-CPE, 1-183 aa), while the C-terminal portion (cCPE, 184–319 aa, 17 kDa) is responsible for interaction with claudin-4 (*19,20*). Taking advantage of the claudin-binding activity of full-length cCPE, Neesse *et al.* fused this fragment to glutathione S-transferase, (cCPE.GST, 41 kDa) and fluorophore Cy5.5 to visualise

claudin-4 overexpression in tumour xenograft and genetically engineered mouse models of pancreatic cancer by near-infrared imaging (*14*). Similarly, Cocco *et al.* used a Fluorescein isothiocyanate (FITC)-conjugated cCPE peptide to successfully measure claudin-4 levels in mouse models of ovarian cancer (*21*). To overcome the limitations associated with optical imaging, as well as antibody-mediated imaging probes (*22*), our group labeled a cCPE.GST conjugate with gamma-emitting radioisotope indium-111 (^{111}In, $t_{1/2}$= 2.8 days) to enable non-invasive whole-body claudin-4 detection in breast cancer mouse models by SPECT imaging. This study confirmed the ability of [^{111}In]In-cCPE.GST to delineate claudin-4 expression both in overt mammary tumours and aplastic lesions in genetically engineered BALB/neuT mice (*23*).

Despite its promise as an early detection tool for claudin-4-overexpressing malignancies, [^{111}In]In-cCPE.GST showed major drawbacks that limit its general utility, such as a moderate claudin-4 binding affinity (in the micromolar range), long circulation half-life and undetermined specificity. In previous studies, a shift in claudin-4 binding properties of the cCPE vector was achieved through structure-based modifications of the C-terminal 223-319 aa region, through a series of point-mutations (*24,25*). Here, we generated a series of smaller-sized mutant cCPE-based radiotracers with the aim of improving the pharmacokinetics and claudin-4 targeting ability of wild-type cCPE, and evaluated these *in vitro* and in *in vivo* mouse models of PDAC.

MATERIALS AND METHODS

Reagents and Cell Lines

Rabbit polyclonal (PA5–28830) and mouse monoclonal (329400) anti-claudin-4 and rabbit polyclonal anti-claudin-3 (341700) antibodies were purchased from ThermoFisher Scientific. Goat anti-mouse horseradish-peroxidase (HRP)-conjugated (5178-2504) and goat anti-rabbit IgG Alexa Fluor® 488 (A11034) antibodies were obtained from Bio-Rad and Invitrogen, respectively. The chelating agent maleimide- diethylenetriamine pentaacetate (DTPA) was purchased from CheMatec (Dijon, France). Water was deionised using a Barnstead NANOpure purification system (Thermo Scientific) and had a resistance of > 18.2 MΩ/cm at 25°C. Protein concentration was measured on a ND-1000 spectrophotometer (NanoDrop Technologies, Inc.). Instant thin-layer chromatography (iTLC) was performed on glass microfiber chromatography paper (Agilent Technologies), and strips were analysed with either a Bioscan AR-2000 radio-TLC scanner (Eckert & Ziegler) or a Cyclone Plus Phosphor Imager (PerkinElmer). Radioactivity measurements were determined using a CRC®-25R dose calibrator (Capintec, Inc.).

PSN-1 (human pancreatic adenocarcinoma) and HT1080 (human connective tissue epithelial fibrosarcoma) cell lines were obtained from the American Type Culture Collection (ATCC). Each of these cell lines was maintained in Dulbecco's Modified Eagle Medium (DMEM), supplemented with 10% fetal bovine serum (FBS), 2 mM L-glutamine, 100 units/mL penicillin, and 0.1 mg/mL streptomycin. HT1080 cells that were stably transfected with human claudin-4 (HT1080/hCLDN-4) were generated as previously described (*26*), and cultured in DMEM (10% FBS, 2 mM L-glutamine, 100 units/mL penicillin, and 0.1 mg/mL streptomycin) supplemented with 5 μg/mL puromycin and 500 μg/mL zeocin. All cells were cultured in a 37°C environment containing 5% CO2. Cells were harvested and passaged as required using trypsin-EDTA solution.

Cells were tested and authenticated by the providers. The cumulative length of culture was less than 6 months following retrieval from liquid nitrogen storage. Cell were tested for the absence of mycoplasma at regular intervals.

Western Blotting

Total cell lysis was performed at 4°C on approximately 1×10^7 cells using RIPA lysis buffer (50 mM Tris, pH 8, 1% NP40, 0.5% sodium deoxycholate, 0.1% sodium dodecyl sulphate, 150 mM sodium chloride, cOmplete™ protease inhibitor cocktail [Sigma-Aldrich]). Cell lysates were isolated by centrifugation after lysis through a 21G hypodermic syringe and 30 s sonication. Thirty microgram lysate samples were run on a 4-12% Bis-Tris MES gel (Novex), transferred to a polyvinylidene difluoride (PVDF) membrane and exposed to a 1:700 dilution of anti-claudin-4 antibody (329400, ThermoFisher Scientific), followed by a 1:3000 dilution of the secondary goat anti-mouse-HRP (5178-2504, Bio-Rad). The blots were developed using Pierce™ ECL Western Blotting Substrate (32106, ThermoFisher Scientific) and exposed to a Li-Cor 3600 Blot scanner.

Immunofluorescence Staining

PSN-1, HT1080, or HT1080/hCLDN4 cells (70,000 cells/well) were seeded onto 8-chamber glass slides (Falcon, Corning, NY USA) and allowed to adhere overnight. Cells, or frozen tumour xenograft sections (10 μm) were washed in PBS and fixed using 4% paraformaldehyde solution (10 min). After washing, the sections were permeabilised using 0.5% digitonin for 15 min at room temperature, washed again and blocked in 2% bovine serum albumen (BSA) for 1 h at room temperature. The cells/sections were then exposed to anti-claudin-4 (PA5-28830; 1:100) or anti-claudin-3 (341700; 1:100) antibody at 4°C overnight, washed in PBS (3 x 5 min) and incubated with goat anti-rabbit IgG Alexa Fluor® 488 (1:500) for 1 h at room temperature. After further

washing (3 x 5 min), slides were mounted using Vectashield with 4′ ,6-diamidino-2-phenylindole (DAPI, Vector H-1200). Fluorescence micrographs were acquired using a Leica TCS SP8 confocal microscope (Leica Microsystems).

Peptide Expression, Modification and Radiolabelling

A C-terminal fragment of CPE (194–319 aa), linked to an H10 fusion protein (H_{10}-$cCPE_{194-319}$) has previously been produced and supplied by Dr Yasuhiko Horiguchi (*27*). H_{10}-$cCPE_{194-319}$ was used as a template for standard site-directed mutagenesis (SDM) methodologies (see supplemental information for additional detail) to make specific amino acid substitutions, which were verified by sequencing of the resulting plasmid (Source BioScience). The modified peptides were expressed in E. coli by isopropyl β- d-1-thiogalactopyranoside (IPTG, MP Biomedicals LLC) addition and purified by affinity chromatography using HisLink^{TM} protein purification resin (Promega). A detailed procedure is laid out in the supplemental data. Purified proteins were dialysed against phosphate-buffered saline (PBS)/2mM ethylenediaminetetraacetic acid (EDTA) at 4°C overnight. Purity of the peptides was confirmed by mass spectroscopy and sodium dodecyl sulfate and polyacrylamide gel electrophoresis (SDS-PAGE) gel followed by Coomassie blue staining.

Purified cCPE peptides were concentrated to 2 mg/mL using an ultrafiltration filter device (Amicon, 3 kDa MW size cut-off, Merck Millipore Ltd.) and incubated with tris(2-carboxyethyl)phosphine hydrochloride (TCEP, 4 mg/mL in water, 3 eq, Cayman Chemical Company) at 25°C, agitating at 300 rpm for 90 min. The peptides were then reacted with maleimide-DTPA (10 mg/mL in DMSO, 5 eq, CheMatech) at 25°C and 300 rpm for 90 min and purified using a Sephadex G-25 resin (Sigma-Aldrich) in sodium citrate buffer (0.1 M, pH 5.5).

DTPA-conjugated peptides were concentrated by centrifugation using 3kDa centrifugal filter units (Millipore).

Indium-111 in 0.02 M hydrochloric acid (Curium Pharma UK Ltd) was added to a 2 mg/mL solution of the DTPA-conjugated cCPE peptides to achieve a 0.1 - 1 MBq/μg molar activity (5.9 - 59 × 10^{-9} GBq/μmol). The reaction mixture was incubated at 37°C for 90 min, and the radiolabelling efficiency was determined by iTLC using an eluent of 50 mM EDTA (pH 5.5). When purification was required, the crude reaction mixture was purified by Sephadex-G25 size exclusion chromatography in PBS (pH 7.4).

Cell Binding Assays

To investigate binding of [^{111}In]In-cCPE peptides to claudin-4 receptors, aliquots of 1.5 x 10^5 PSN-1, expressing claudin-4, and HT1080, not expressing claudin-3 or -4, and HT1080/hCLDN4, only expressing claudin-4, were seeded onto a 24-well plate in 500 μL of growth medium and allowed to adhere overnight. Cells were then incubated with increasing amount (0.5-160 nM) of [^{111}In]In-DTPA-cCPE (1 MBq/μg) for 2 h at 4°C. After incubation, supernatant was removed and cells were washed and lysed using 0.1 M sodium hydroxide. ^{111}In radioactivity in the cell-associated fractions was measured using an automated gamma-counter (Wizard^2 2480, Perkin Elmer) and normalised by the amount of protein present in the seeding controls determined by bicinchoninic acid (BCA) assay. Binding affinity (K_D) was estimated by non-linear regression analysis with a one-site total binding model using the software package GraphPad Prism v7 (GraphPad Software Inc).

In Vivo Studies

All animal procedures were performed in accordance with the UK Animals (Scientific Procedures) Act 1986 and with local ethical committee approval.

In vivo imaging experiments were performed using a VECTor^{4}CT SPECT/ computerised tomography (CT) system (MILabs, Utrecht, The Netherlands). For dynamic SPECT imaging, male BALB/c mice (n=3) were anesthetized by 4% isoflurane gas (0.5 L/min O_2) and placed on a custom-built imaging cradle in a prone position. Animals were intravenously injected with [^{111}In]In-cCPE$_{194-319}$ (5 µg, 5 MBq, <200µL) through a tail vein catheter, and dynamic imaging was performed over 90 min after tracer administration. SPECT data was acquired (150 frames, 30 s per frame, 2.1 s per bed position using list mode acquisition) using an ultra-high resolution rat/mouse 1.8 mm collimator, followed by a cone-beam CT scan (55 kV, 0.19 mA, 20 ms) for anatomical reference and attenuation correction. Anaesthesia was maintained at 2.5 % isoflurane and body temperature was kept at 37°C throughout the duration of the scan. SPECT images were reconstructed using U-SPECT-Rec3.22 software (MILabs, Utrecht, The Netherlands), applying a pixel-based algorithm with 8 subsets, 6 iterations and 0.8 mm^3 voxel size for ^{111}In (energy window of 159-278 keV, background weight 2.5).

To allow quantification of SPECT data, calibration factors derived from ^{111}In phantoms were used. SPECT images were registered to their corresponding CT and attenuation corrected. Quantification of SPECT images using volume-of-interest (VOI) analyses was performed using the PMod software package (Version 3.807, PMOD Technologies), to calculate the percentage of the injected dose per millilitre per VOI (%ID/mL) per time bin.

After imaging, mice were euthanised by cervical dislocation, and organs of interest were excised and weighed. The amount of radioactivity in each organ was measured using a WIZARD^2 2470 gamma counter (PerkinElmer). Counts per minute were converted to MBq using a calibration curve generated from known standards. All values were decay-corrected to the time of injection, and the percentage of the injected dose per gram (%ID/g) of each sample was calculated.

Tumours were generated in BALB/c *nu/nu* mice, by subcutaneous injection of 10^6 cells in DMEM. Tumours were allowed to grow for 3-4 weeks. Animals were used for subsequent studies when the tumour reached 200 mm^3. Static SPECT images were acquired after intravenous administration of ^{111}In-labelled cCPE peptides (5 μg, 5 MBq) in sterile 0.9% saline (<200 μL) were injected intravenously *via* the lateral tail vein (n = 3/peptide/cell line). SPECT/CT images were acquired at 90 min post-injection of the tracer over 7 min using a 1.8 mm pinhole rat collimator (3 frames, 2.3 min/frame, 11.5 s/bed position).

Ex Vivo

After imaging, tumour xenografts were flash-frozen in isopentane (Sigma-Aldrich) chilled with liquid nitrogen and stored at -80°C overnight. Frozen tissue was sectioned (10 μm) using an OTF5000 cryotome (Bright Instruments Ltd). Tissue sections were thaw-mounted onto Superfrost PLUS glass microscope slides (Menzel-Glaser, Thermo Scientific) and allowed to dry at room temperature. The slides were then exposed to a storage phosphor screen (PerkinElmer, Super Resolution, 12.5 × 25.2 cm) for 15 h. The phosphor screen was then imaged using a Cyclone® Plus Storage Phosphor System (PerkinElmer).

Statistical Analyses

All statistical analyses and non-linear regression were performed using GraphPad Prism (GraphPad Software Inc). One-way ANOVA was used for multiple comparisons, with Tukey post-tests to calculate significance of differences between groups. All data were obtained as triplicate independent replicates. Results are reported and graphed as averages ± one standard deviation, unless stated otherwise.

RESULTS

Claudin-4 Expression in Human Pancreatic Cancer Cell Lines

Eight pancreatic cell lines of human origin were analysed by western blot for claudin-4 expression (Fig. 1A). Claudin-4 was found to be expressed in 7 out of 8 cell lines, with the highest levels in the human pancreatic adenocarcinoma Capan-2 cells and the lowest in the human pancreatic epithelial carcinoma Mia-PaCa-2 cells. No claudin-4 expression was detectable by western blot in the human pancreatic carcinoma FAMPAC-1 cells or the human fibrosarcoma HT1080 cell line. The latter served as negative control in this study. Due to their fast growth rate and ability to establish robust and reproducible subcutaneous tumour xenografts in mice, PSN-1 cells were selected among all claudin-4-expressing PDAC cell lines for further experiments (*28*).

The presence of claudin-4 in PSN-1 cells was also confirmed by fluorescence immunocytochemistry (Fig. 1B). Claudin-4 protein was found to be localised at the cell-cell contacts and associated with intracellular vesicles in confluent PSN-1 cells, but not in HT1080 cells. In PDAC sections harvested from patients, claudin-4 is expressed strongly at the cell membrane (*29*).

Design and Synthesis of cCPE-based Radiotracers

To improve the pharmacokinetics and claudin-4 binding properties of [^{111}In]In-cCPE.GST, five smaller-sized variants were generated, using structural proteomic and recombinant protein expression methodologies (Supplemental Fig. 1) (18). Based on the crystal structure of cCPE, and the knowledge that residues 290-319 are necessary for claudin binding, specific amino acid substitutions were introduced to the wild type sequence (194-319 aa) by site-directed mutagenesis in order to enhance the affinity (S313A and S307A+N309A+S313A) or specificity (D284A and

L254F+K257D) of cCPE for claudin-4 (*20,30*). While some mutations had previously been reported in the literature, the L254F+K257D modification was predicted through molecular docking modelling of the interaction between the cCPE binding site, claudin-4, and a number of closely related claudins (claudin-3 and claudin-19) (Supplemental Fig. 1) (*24,25*). Additionally, a single cysteine residue was added to the sequence to allow site-specific conjugation of the peptide to a maleimide-DTPA chelator. Furthermore, ten amino acids of wild-type cCPE (184-193 aa) were removed from the vector as they were found not to be crucial for claudin-4-targeting (*20*). Together, these changes led to a reduction in size from 41 to 17 kDa, with the aim to produce more rapid pharmacokinetics and allow faster imaging. A plasmid vector expressing the $cCPE_{194-319}$ fragment linked to an H10 fusion protein for purification, instead of the far larger GST fusion protein, was used as a template for modifications induced by site-directed mutagenesis, which were verified by sequencing (Supplemental Fig. 1).

All plasmids, encoding for wild-type or mutant cCPE.histidine (his)10 sequences, were introduced into competent E. coli BL21(DE3) cells. Protein expression was induced via IPTG addition and the resulting peptides were purified by nickel affinity chromatography and dialysis (Fig. 1C), and characterised by mass spectroscopy (Supplemental Fig 2). After modification with maleimide-DTPA, all cCPE peptides were radiolabelled with ^{111}In with excellent radiochemical yield (>99%) and purity (>99%), and a typical molar activity of 1 MBq/µg (Fig. 1D).

In Vitro Characterisation

All radiolabelled peptides bound claudin-4-expressing PSN-1 cells in a saturable manner, but not claudin-4-negative HT1080 control cells (Fig. 2A). After exposure of cells to radiolabelled cCPE peptides at saturation concentration (40 nM) for 2 h, radioactivity associated with PSN-1 cells was

approximately nine times higher compared to HT1080 cells ($P<0.0001$). Saturation binding assays yielded affinities (K_D) in the nanomolar range (2.2-10.2 nM) for all labelled cCPE-based peptides, a marked improvement over earlier reported values in the micromolar range for unmodified CPE binding to purified His_{10}-claudin-4 or [^{111}In]In-cCPE.GST binding to claudin-4-expressing human mammary gland/breast epithelial MDA-MB-468 cells (0.65 and 1.93 μM, respectively (*14,23*)). The wildtype $cCPE_{194-319}$, S313A, and S307A+N309A+S313A variants showed the better binding affinity in PSN-1 cells (K_D 2.2 ± 0.8, 3 ± 0.1 and 4.2 ± 0.5 nM, respectively) while the D284A and L254F+K257D mutants showed higher K_D values (10 ± 0.9 and 9.7 ± 0.7 nM, respectively) (Fig. 2B).

To evaluate the specificity of these radiolabelled cCPE peptides for claudin-4 receptors, we performed *in vitro* blocking studies, by adding increasing amounts of cold, unlabelled cCPE.GST (100-fold) (Fig. 3). In addition to PSN-1 cells, we used the HT1080-hCLDN4 cell line, stably transfected with human claudin-4 and lacking expression of claudin-3, a closely related claudin protein. We confirmed strong vesicular and membranar claudin-4 immunostaining, but absence of claudin-3 signal in HT1080-hCLDN4 cells (Fig. 3). Efficient blocking (>95%, all $P<0.001$) of ^{111}In-labelled $cCPE_{194-319}$, S313A, and S307A+N309A+S313A was achieved by addition of a 100-fold excess of cCPE.GST in both PSN-1 and HT1080-hCLDN4, suggesting a highly specific interaction of these cCPE variants and claudin-4, and other potential binding epitopes of cCPE, with very little non-specific uptake. Cell-associated uptake of [^{111}In]In-$cCPE^{D284A}$ could only be blocked by 85% in both cell lines ($P<0.001$), while the ^{111}In-$cCPE^{L254F+K257D}$ mutant showed the lowest specificity of all peptides, with only 38% blocking achieved in PSN-1 cells and 74% in HT1080-hCLDN4 cells ($P<0.001$).

For additional cross-validation of the radiolabelled cCPE^{S313A}, this variant was also fluorescently labelled using a Cy5 maleimide dye. PSN-1 cells were exposed to Cy5-labelled cCPE^{S313A}, and subsequently imaged by confocal microscopy (Supplemental Fig. 3). The fluorescence associated with Cy5-cCPE^{S313A} was localised mainly in the cytoplasm and plasma membrane of PSN-1 cells, similar to claudin-4 immunostaining.

In Vivo Imaging

Initial *in vivo* evaluation of our tracer design was performed in wildtype mice using the ^{111}In-radiolabelled wildtype cCPE$_{194-319}$ variant to determine pharmacokinetics. Otherwise naïve BALB/c mice were injected intravenously with the tracer via a tail vein catheter and imaged dynamically by SPECT over 75 min. The radiopeptide cleared very rapidly from blood, following a mono-exponential decay pattern with a half-life of 0.5 ± 0.2 min, as measured by image VOI analysis on kinetic SPECT images (Supplemental Fig. 4). Both SPECT imaging and *ex vivo* gamma-counting revealed high accumulation of the radiopeptide in the kidneys, liver and salivary glands (32.9 ± 6.7, 25.3 ± 5.8 and 6.3 ± 2.1 %ID/mL at 75 min post-injection, respectively). Elimination of [^{111}In]In-cCPE$_{194-319}$, occurred through renal and hepatic routes.

The feasibility of claudin-4-targeted tumour detection *in vivo* with wild-type versus mutant cCPE-based radiotracers was then assessed in immuno-compromised mice bearing subcutaneous PSN-1 or HT1080 tumour xenografts (Fig. 4). All mice were injected intravenously with cCPE radiotracer (n=3/peptide/cell line) and imaged by SPECT/CT at 90 min post-administration, to ensure that most radioactivity had cleared from blood. *Ex vivo* counting of organs and tissues at 90 min post-injection showed significantly higher accumulation of all cCPE-based radiotracers in claudin-4 expressing PSN-1 tumour xenografts when compared with HT1080 controls ([^{111}In]In-

cCPE$_{194-319}$: 2.7 ± 0.8 vs 0.4 ± 0.1 %ID/g, P<0.001; [^{111}In]In-cCPE^{S313A}: 2.3 ± 0.9 vs 0.5 ± 0.1 %ID/g, P<0.01; [^{111}In]In-cCPE$^{S307A+N309A+S313A}$: 2 ± 0.4 vs 0.3 ± 0.1 %ID/g, P<0.01; [^{111}In]In-cCPE^{D284A}: 2 ± 0.2 vs 0.7 ± 0.1 %ID/g, P<0.05; [^{111}In]In-cCPE$^{L254F+K257D}$: 6.3 ± 0.9 vs 0.7 ± 0.2 %ID/g, P<0.001) (Fig. 4B). [^{111}In]In-cCPE$^{L254F+K257D}$ exhibited the highest uptake in PSN-1 tumour tissue, nearly 3-fold greater than average tumour uptake of the other labelled compounds tested here, and similar to that previously reported for [^{111}In]In-cCPE.GST in MDA-MB-468 xenografts at 24 h post-administration of the tracer (6.72 ± 0.18 %ID/g) (*23*). *Ex vivo* autoradiography of xenograft sections corroborated higher tracer uptake in PSN-1 tumours than HT1080 xenografts. Immunofluorescence imaging confirmed claudin-4 overexpression in PSN-1, but not in HT1080 tumour xenografts (Fig. 4C).

As expected, tracer clearance from blood was fast, resulting in good tumour-to-blood ratios in PSN-1 xenograft-bearing mice at 90 min post-injection of the tracer, all significantly higher when compared to claudin-4-negative controls except for [^{111}In]In-cCPE$^{S307A+N309A+S313A}$ ([^{111}In]In-cCPE$_{194-319}$: 1.7 ± 0.3 vs 0.3 ± 0.1, P<0.01; [^{111}In]In-cCPE^{S313A}: 1.7 ± 0.8 vs 0.3 ± 0.1, P<0.01; [^{111}In]In-cCPE$^{S307A+N309A+S313A}$: 1.4 ± 0.2 vs 0.7 ± 0.7, P>0.05; [^{111}In]In-cCPE^{D284A}: 4.3 ± 0.2 vs 0.6 ± 0.2, P<0.001; [^{111}In]In-cCPE$^{L254F+K257D}$: 2.2 ± 0.2 vs 0.5 ± 0.1, P<0.001). Tumour-to-muscle ratios were excellent for all radiopeptides, with [^{111}In]In-cCPE^{D284A} and [^{111}In]In-cCPE$^{L254F+K257D}$ showing the best contrast with respect to HT1080 tumour xenografts ([^{111}In]In-cCPE$_{194-319}$: 6.2 ± 1.5 vs 1.2 ± 0.3, P<0.001; [^{111}In]In-cCPE^{S313A}: 3.8 ± 1.2 vs 0.9 ± 0.2, P<0.01; [^{111}In]In-cCPE$^{S307A+N309A+S313A}$: 3.4 ± 0.6 vs 0.7 ± 0.1, P<0.05; [^{111}In]In-cCPE^{D284A}: 7.4 ± 1 vs 1.5 ± 0.3, P<0.001; [^{111}In]In-cCPE$^{L254F+K257D}$: 10 ± 1.1 vs 1.4 ± 0.5, P<0.001). Although tracer uptake in blood and muscle was low, all radiotracers displayed prominent renal and hepatic retention in both xenograft models, which limited overall image contrast. Among all peptides, [^{111}In]In-

cCPE^{D284A} and [^{111}In]In-cCPE$^{L254F+K257D}$ showed the lowest accumulation in the liver (PSN-1: 11.5 ± 1.4 and 12.5 ± 1.4 %ID/g) and kidneys (PSN-1: 37.1 ± 5.5 and 36.1 ± 1.7 %ID/g) when compared to [^{111}In]In-cCPE$_{194-319}$ (liver: 38.7 ± 0.9 %ID/g; kidneys: 171.2 ± 12.9 %ID/g), [^{111}In]In-cCPE^{S313A} (liver: 62.2 ± 4.2 %ID/g; kidneys: 130.9 ± 3.6 %ID/g) and [^{111}In]In-cCPE$^{S307A+N309A+S313A}$ (liver: 58.5 ± 5.4 %ID/g; kidneys: 140.2 ± 13 %ID/g) (Fig. 4D).

DISCUSSION

Tight junction dysfunction is an important hallmark of epithelial carcinomas and plays a key role in tumour growth and metastatic progression. Claudin-4 overexpression is a common signature of this process and is considered a promising biomarker for cancer detection and prognosis in a variety of cancer types. Claudin-4's role in pathogenesis is yet to be fully elucidated, it has been targeted for molecular imaging with both anti-claudin-4 antibodies and CPE-based peptides, a means for speeding up diagnosis, stratifying patients into risk groups and even assessing response to therapy (*31,32*). A claudin-4 imaging agent might also be a useful tool for monitoring the effects of claudin-4-targeted therapies, which have shown promise in suppressing tumour growth in several preclinical cancer models (*31,33,34*). Neesse et al. first used a fluorescently labelled cCPE.GST peptide for detection of pancreatic cancer (*14*), and Cocco et al. investigated fluorescently labelled small cCPE-based peptides for intraoperative imaging (*21*). We previously reported on the characterisation of a radiolabelled anti-Claudin-4 antibody (*22*). An in-depth validation of these claudin-targeting compounds is not always systematically performed, making comparison of characteristics more challenging. cCPE-based imaging agents offer the advantage of faster clearance rates and shorter acquisition times with respect to anti-claudin-4 antibodies. Several studies have reported the use of this toxin fragment to measure claudin-4 levels non-invasively. We previously radiolabelled a cCPE.GST peptide with ^{111}In to enable SPECT imaging

of claudin-4 in mouse models of breast cancer (*23*). Although targeted imaging was achieved, this probe showed only modest target binding affinity and specificity. Hence, improving the binding properties of cCPE for claudin-4 receptors is required prior to clinical translation.

The compounds described herein, a combination of previously described empirically validated enabling mutations and de novo designed variants, show a much improved combination of pharmacokinetics and affinity, than previous radiolabelled claudin-4-targeting imaging agents (*22,23*). The affinity of the novel radiolabelled cCPE.his$_{10}$ proteins, measured *in vitro* was consistently stronger when compared to [^{111}In]In-cCPE.GST in MDA-MB-468 cells, in the low nanomolar versus low micromolar range, possibly because of a different presentation of the claudin-binding domain, although there was little affinity advantage over anti-claudin-4 IgG. The lack of a bulky GST tag also resulted in far faster elimination from blood, allowing *in vivo* imaging after a few hours, rather than 1-3 days. Compared to an IgG, production of small cCPE proteins is far more economical. In addition, the smaller size of the his10 series may provide improved access to claudin-4, expressed in the tight spaces between cells, increasing target epitope availability. This may also explain the high uptake in the intestines of the cCPE.his10 series, compared to its bulkier variants, as they have better access to the claudin epitopes that are expressed on the luminal side of the intestinal lining.

Point mutations in the claudin epitope-binding domain significantly influenced claudin-4 affinity, although effects were minimal apart from the D284A variant. Mutational changes more profoundly influenced pharmacokinetics and selectivity. Whereas the uptake of wild type cCPE and the S313A and triple mutants in Claudin-4-expressing cell lines could be blocked with an excess of cCPE.GST, this was not true to the same extent for D284A and L254F/K257D, indicating they may have a different selectivity profile. Regarding kinetics, notably the D284A showed far

faster blood clearance (with blood values at 90 min post injection up to 3-fold lower compared to other compounds), resulting in consistently lower normal tissue and intestinal uptake. Both D284A and L254F+K257D variants show lower liver accumulation. This resulted in improved tumour-to-blood and tumour-to-liver ratios. Hepatic expression of claudin-4 is low, compared to tumour, although claudin-3 expression is not insignificant (*35*), and may play a role in the differences we have observed. Taken together, these results highlight that small changes in the cCPE sequence can thus result in large changes in pharmacokinetic behaviour, and each novel cCPE-based compound should therefore be fully characterised. Some of the disadvantages of our approach include protein production, which was variable between clones and between batches, and therefore would benefit from optimisation. To improve the pharmacokinetic profile of the new cCPE-based probes, the composition and position of the polyhistidine-tag could be changed in order to further reduce non-specific uptake (*36,37*). The selection of a different chelator may also increase tumour-to-background contrast and might be indicated if a shorter-lived radioisotope is chosen in view of the fast pharmacokinetics of the cCPE peptides (*38*).

The work presented here provides a proof-of-principle for optimisation of cCPE-based imaging agents, based on point mutations of the wildtype sequence. Possible applications include their use as diagnostic tools for PET or SPECT, intraoperative fluorescence imaging agents, or tumour-targeting vectors.

CONCLUSION

[^{111}In]In-cCPE mutants are a useful tool for non-invasive imaging of claudin-4 which is a widely dysregulated and highly prognostic biomarker in pancreatic cancer. These imaging agent could

therefore be used to aid in the early detection and characterisation of this malignancy, among other applications.

ACKNOWLEDGEMENTS

This research was supported financially by the CRUK/MRC Oxford Institute for Radiation Oncology (MM, VK, BC), MRC (SK), Pancreatic Cancer UK (SH) and Pancreatic Cancer Research Fund (JBT). AC and SK are are grateful for support by the SGC, a registered charity (number 1097737) that receives funds from AbbVie, Bayer Pharma AG, Boehringer Ingelheim, Canada Foundation for Innovation, Eshelman Institute for Innovation, Genome Canada, Innovative Medicines Initiative (EU/EFPIA), Janssen, Merck KGaA, Germany, MSD, Novartis Pharma AG, Ontario Ministry of Economic Development and Innovation, Pfizer, São Paulo Research Foundation-FAPESP, Takeda, and Wellcome.

Competing Financial Interests

The authors declare that they have no conflicting interests.

Key Points

QUESTION: Radiolabelled cCPE proteins can be used for imaging claudin. We investigated whether optimisation of the sequence and structure can lead to improved characteristics of this radiopharmaceutical.

PERTINENT FINDINGS: We found that truncated, smaller and mutant versions of labelled cCPE demonstrated superior binding affinity and improved pharmacokinetics compared to previously reported compounds.

IMPLICATIONS FOR PATIENT CARE: Optimization of the cCPE sequence may lead to improved detection of claudin-4 expressing cancers.

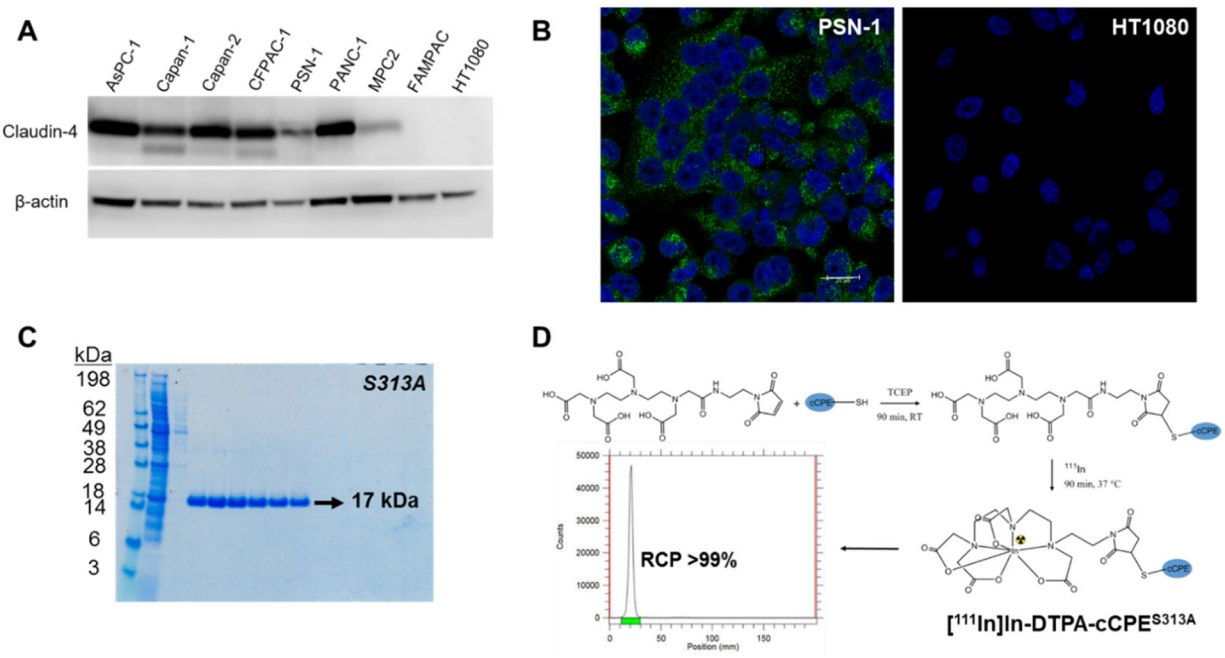

***Figure 1*:** A) Claudin-4 expression in a panel of human pancreatic cancer cell lines detected by western blot. B) Immunofluorescence staining of claudin-4 expression in human PDAC PSN-1 cell line and claudin-4 non-expressing HT1080 fibrosarcoma cells. (Green: claudin-4; blue: DAPI, represents cell nuclei; Scale bar represents 20 μm). C) Coomassie Blue stained SDS-PAGE gel of purified S313A variant. All peptides were obtained with >95% purity. D) Schematic representation of bioconjugation and ^{111}In radiolabelling strategies for cCPE mutants. cCPE peptides were initially reduced with TCEP and site-specifically conjugated to maleimide-DTPA. The resulting bioconjugates were radiolabelled with ^{111}In with excellent radiochemical purity (>99%) and yield (>95%).

A

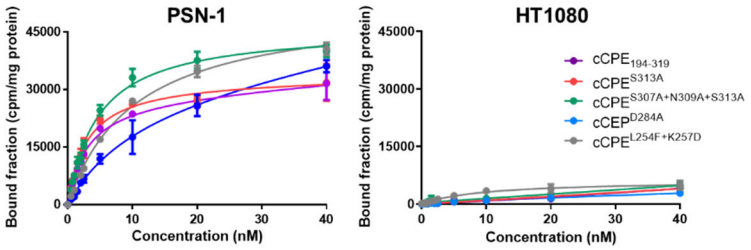

B

K_D (nM)	PSN-1	HT1080
$cCPE_{194-319}$	3.0 ± 0.1	>100
$cCPE^{S313A}$	2.2 ± 0.8	>100
$cCPE^{S307A+N309A+S313A}$	4.2 ± 0.5	>100
$cCPE^{D284A}$	10.2 ± 0.9	>100
$cCPE^{L254F+K257D}$	9.7 ± 0.7	>100

***Figure 2*:** A) PSN-1 and HT1080 cells were exposed for 2 h at 4°C to increasing concentrations of ^{111}In-labeled cCPE peptides, and extent of cell-binding was determined. B) Experimental results for all tested cCPE radiopeptides in PSN-1 and HT1080 cells.

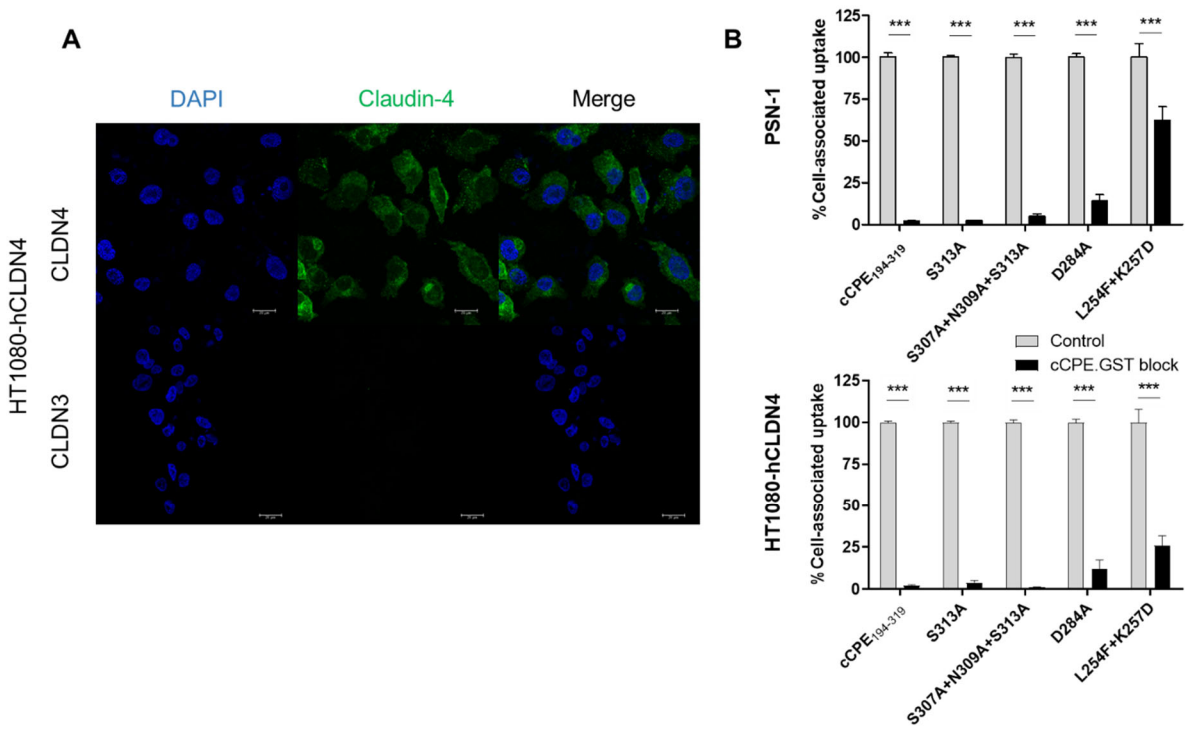

***Figure 3*:** A) Immunocytochemistry of claudin-4 (top) and claudin-3 (bottom) in HT1080 cells stably transfected with human claudin-4 (HT1080-hCLDN4). Green fluorescence indicates claudin-4 positive staining, and blue (DAPI) fluorescence indicates cell nuclei. Scale bar indicates 20 µm. B) An excess of cold, unlabelled cCPE.GST (100-fold) was used to block binding of cCPE radiopeptides to PSN-1 (top) and HT1080-hCLDN4 (bottom) cells. *** P<0.001.

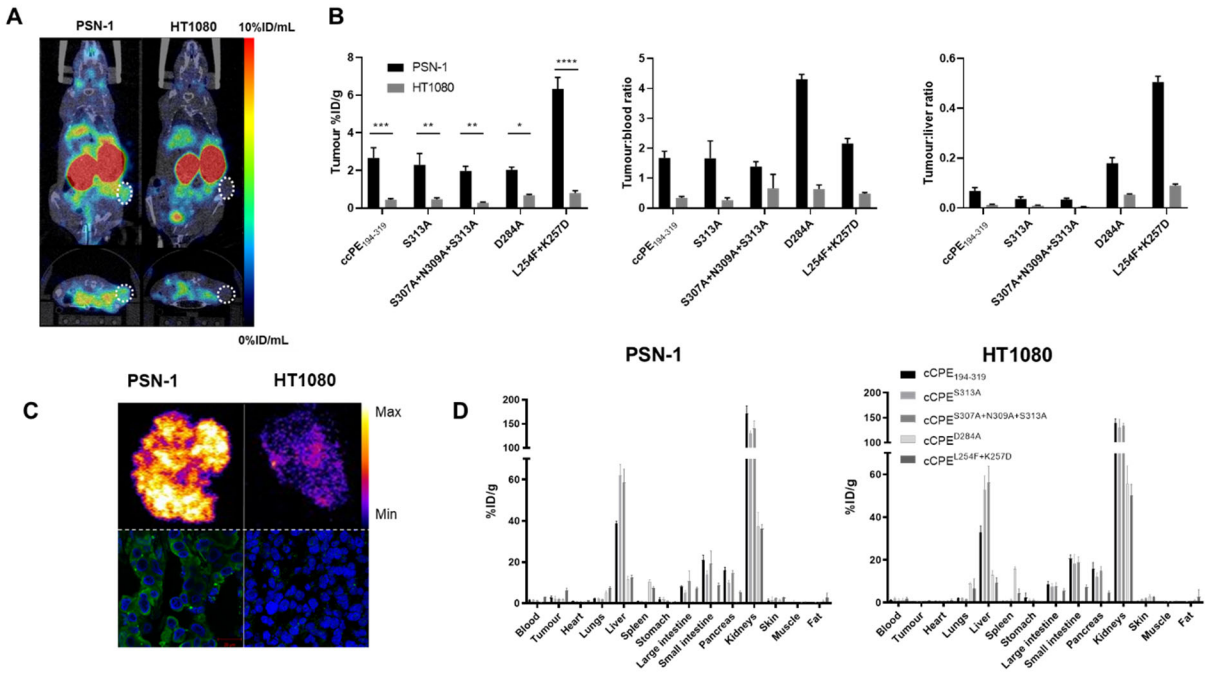

***Figure 4*:** A) Representative SPECT/CT images of mice carrying tumour xenografts (white circles) of PSN-1 (claudin-4–positive) or HT1080 (claudin-4–negative) cells 90 min after intravenous injection of [^{111}In]In-cCPE$^{L254F+K257D}$. Coronal and axial sections through tumour are shown. B) *Ex vivo* tumour uptake (%ID/g), tumour-to-blood and tumour-to-liver ratios of ^{111}In-radiolabelled cCPE peptides 2 h after intravenous administration of the tracer. *=p<0.05; **=P<0.01; ***=P<0.001. C) Autoradiography images of PSN-1 and HT1080 tumour xenograft sections of mice injected with [^{111}In]In-cCPE$^{L254F+K257D}$ and corresponding confocal images of immunofluorescence staining of claudin-4 (green=claudin-4; blue=DAPI. Scale bar represents 20 µm). PSN-1 tumour sections showed significantly higher tracer uptake compared to negative control. D) Biodistribution of ^{111}In-radiolabelled cCPE peptides 2 h after intravenous administration of the tracer.

REFERENCES

1. Collaborators GBDPC. The global, regional, and national burden of pancreatic cancer and its attributable risk factors in 195 countries and territories, 1990-2017: a systematic analysis for the Global Burden of Disease Study 2017. *Lancet Gastroenterol Hepatol.* 2019;4:934-947.

2. Howlader N NA, Krapcho M, Miller D, Brest A, Yu M, Ruhl J, Tatalovich Z, Mariotto A, Lewis DR, Chen HS, Feuer EJ, Cronin KA (eds). SEER Cancer Statistics Review, 1975-2016, National Cancer Institute. *SEER Cancer Statistics Review,.* 2019.

3. Ghaneh P, Hanson R, Titman A, et al. PET-PANC: multicentre prospective diagnostic accuracy and health economic analysis study of the impact of combined modality 18fluorine-2-fluoro-2-deoxy-d-glucose positron emission tomography with computed tomography scanning in the diagnosis and management of pancreatic cancer. *Health Technol Assess.* 2018;22:1-114.

4. Higashi T, Saga T, Nakamoto Y, et al. Diagnosis of pancreatic cancer using fluorine-18 fluorodeoxyglucose positron emission tomography (FDG PET) --usefulness and limitations in "clinical reality". *Ann Nucl Med.* 2003;17:261-279.

5. Xu HX, Chen T, Wang WQ, et al. Metabolic tumour burden assessed by (1)(8)F-FDG PET/CT associated with serum CA19-9 predicts pancreatic cancer outcome after resection. *Eur J Nucl Med Mol Imaging.* 2014;41:1093-1102.

6. Wilson JM, Mukherjee S, Brunner TB, Partridge M, Hawkins MA. Correlation of (18)F-Fluorodeoxyglucose Positron Emission Tomography Parameters with Patterns of Disease Progression in Locally Advanced Pancreatic Cancer after Definitive Chemoradiotherapy. *Clin Oncol (R Coll Radiol).* 2017;29:370-377.

7. Knight JC, Mosley MJ, Bravo LC, et al. (89)Zr-anti-gammaH2AX-TAT but not (18)F-FDG Allows Early Monitoring of Response to Chemotherapy in a Mouse Model of Pancreatic Ductal Adenocarcinoma. *Clin Cancer Res.* 2017;23:6498-6504.

8. Segard T, Robins PD, Yusoff IF, et al. Detection of hypoxia with 18F-fluoromisonidazole (18F-FMISO) PET/CT in suspected or proven pancreatic cancer. *Clin Nucl Med.* 2013;38:1-6.

9. Lamarca A, Asselin MC, Manoharan P, et al. 18F-FLT PET imaging of cellular proliferation in pancreatic cancer. *Crit Rev Oncol Hematol.* 2016;99:158-169.

10. Kwon MJ. Emerging roles of claudins in human cancer. *Int J Mol Sci.* 2013;14:18148-18180.

11. Turksen K, Troy TC. Junctions gone bad: claudins and loss of the barrier in cancer. *Biochim Biophys Acta.* 2011;1816:73-79.

12. Martin TA. The role of tight junctions in cancer metastasis. *Semin Cell Dev Biol.* 2014;36:224-231.

13. Nichols LS, Ashfaq R, Iacobuzio-Donahue CA. Claudin 4 protein expression in primary and metastatic pancreatic cancer: support for use as a therapeutic target. *Am J Clin Pathol.* 2004;121:226-230.

14. Neesse A, Hahnenkamp A, Griesmann H, et al. Claudin-4-targeted optical imaging detects pancreatic cancer and its precursor lesions. *Gut.* 2013;62:1034-1043.

15. Michl P, Barth C, Buchholz M, et al. Claudin-4 expression decreases invasiveness and metastatic potential of pancreatic cancer. *Cancer Res.* 2003;63:6265-6271.

16. Tsutsumi K, Sato N, Tanabe R, et al. Claudin-4 expression predicts survival in pancreatic ductal adenocarcinoma. *Ann Surg Oncol.* 2012;19 Suppl 3:S491-499.

17. Shang X, Lin X, Alvarez E, Manorek G, Howell SB. Tight junction proteins claudin-3 and claudin-4 control tumor growth and metastases. *Neoplasia.* 2012;14:974-985.

18. Lin X, Shang X, Manorek G, Howell SB. Regulation of the Epithelial-Mesenchymal Transition by Claudin-3 and Claudin-4. *PLoS One.* 2013;8:e67496.

19. Michl P, Buchholz M, Rolke M, et al. Claudin-4: a new target for pancreatic cancer treatment using Clostridium perfringens enterotoxin. *Gastroenterology.* 2001;121:678-684.

20. Van Itallie CM, Betts L, Smedley JG, 3rd, McClane BA, Anderson JM. Structure of the claudin-binding domain of Clostridium perfringens enterotoxin. *J Biol Chem.* 2008;283:268-274.

21. Cocco E, Casagrande F, Bellone S, et al. Clostridium perfringens enterotoxin carboxy-terminal fragment is a novel tumor-homing peptide for human ovarian cancer. *BMC Cancer.* 2010;10:349.

22. Torres JB, Knight JC, Mosley MJ, et al. Imaging of Claudin-4 in Pancreatic Ductal Adenocarcinoma Using a Radiolabelled Anti-Claudin-4 Monoclonal Antibody. *Mol Imaging Biol.* 2018;20:292-299.

23. Mosley M, Knight J, Neesse A, et al. Claudin-4 SPECT Imaging Allows Detection of Aplastic Lesions in a Mouse Model of Breast Cancer. *J Nucl Med.* 2015;56:745-751.

24. Veshnyakova A, Piontek J, Protze J, Waziri N, Heise I, Krause G. Mechanism of Clostridium perfringens enterotoxin interaction with claudin-3/-4 protein suggests structural modifications of the toxin to target specific claudins. *J Biol Chem.* 2012;287:1698-1708.

25. Takahashi A, Komiya E, Kakutani H, et al. Domain mapping of a claudin-4 modulator, the C-terminal region of C-terminal fragment of Clostridium perfringens enterotoxin, by site-directed mutagenesis. *Biochem Pharmacol.* 2008;75:1639-1648.

26. Li X, Iida M, Tada M, et al. Development of an anti-claudin-3 and -4 bispecific monoclonal antibody for cancer diagnosis and therapy. *J Pharmacol Exp Ther.* 2014;351:206-213.

27. Katahira J, Sugiyama H, Inoue N, Horiguchi Y, Matsuda M, Sugimoto N. Clostridium perfringens enterotoxin utilizes two structurally related membrane proteins as functional receptors in vivo. *J Biol Chem.* 1997;272:26652-26658.

28. Wilson TC, Xavier MA, Knight J, et al. PET Imaging of PARP Expression Using (18)F-Olaparib. *J Nucl Med.* 2019;60:504-510.

29. Uhlen M, Zhang C, Lee S, et al. A pathology atlas of the human cancer transcriptome. *Science.* 2017;357.

30. Hanna PC, Mietzner TA, Schoolnik GK, McClane BA. Localization of the receptor-binding region of Clostridium perfringens enterotoxin utilizing cloned toxin fragments and synthetic peptides. The 30 C-terminal amino acids define a functional binding region. *J Biol Chem.* 1991;266:11037-11043.

31. Neesse A, Griesmann H, Gress TM, Michl P. Claudin-4 as therapeutic target in cancer. *Arch Biochem Biophys.* 2012;524:64-70.

32. Cornelissen B, Knight JC, Mukherjee S, et al. Translational molecular imaging in exocrine pancreatic cancer. *Eur J Nucl Med Mol Imaging.* 2018;45:2442-2455.

33. Hashimoto Y, Kawahigashi Y, Hata T, et al. Efficacy and safety evaluation of claudin-4-targeted antitumor therapy using a human and mouse cross-reactive monoclonal antibody. *Pharmacol Res Perspect.* 2016;4:e00266.

34. Maeda T, Murata M, Chiba H, et al. Claudin-4-targeted therapy using Clostridium perfringens enterotoxin for prostate cancer. *Prostate.* 2012;72:351-360.

35. Huttlin EL, Jedrychowski MP, Elias JE, et al. A tissue-specific atlas of mouse protein phosphorylation and expression. *Cell.* 2010;143:1174-1189.

36. Vorobyeva A, Schulga A, Konovalova E, et al. Optimal composition and position of histidine-containing tags improves biodistribution of (99m)Tc-labeled DARPin G3. *Sci Rep.* 2019;9:9405.

37. Hofstrom C, Altai M, Honarvar H, et al. HAHAHA, HEHEHE, HIHIHI, or HKHKHK: influence of position and composition of histidine containing tags on biodistribution of [(99m)Tc(CO)3](+)-labeled affibody molecules. *J Med Chem.* 2013;56:4966-4974.

38. Mitran B, Varasteh Z, Selvaraju RK, et al. Selection of optimal chelator improves the contrast of GRPR imaging using bombesin analogue RM26. *Int J Oncol.* 2016;48:2124-2134.

Supplementary information

cCPE Peptides for SPECT Imaging of Claudin-4 Overexpression in Pancreatic Cancer

Julia Baguña Torres[1], Michael Mosley[1], Sofia Koustoulidou[1], Samantha Hopkins[1], Stefan Knapp[2,3], Apirat Chaikuad[2], Masuo Kondoh[4], Keisuke Tachibana[4], Veerle Kersemans[1] and Bart Cornelissen[1*]

[1] Cancer Research UK and Medical Research Council Oxford Institute for Radiation Oncology, University of Oxford, UK

[2] Institute of Pharmaceutical Chemistry and Structure Genomics Consortium (SGC), Goethe-University Frankfurt, 60438 Frankfurt am Main, Germany

[3] German Cancer Network (DKTK), site Mainz-Frankfurt

[4] Graduate School of Pharmaceutical Sciences, Osaka University, 1-6 Yamadaoka, Suita, Osaka, 565-0871, Japan

Supplementary information

Construction of cCPE site-directed mutagen plasmids

This study involved the modification of the peptide sequence of cCPE in an attempt to improve its affinity and selectivity for the Claudin-4 target molecule. The DNA clone template used to produce the point-mutation forms was a cCPE-HIS plasmid (pETH10PER), comprising the COOH-terminal fragment of CPE (aa 184–319) linked to a HIS fusion peptide, generated and supplied by Yasuhiko Horiguchi (*1*).

First, we produced a 194-319 fragment, removing the N-terminal 10 amino-acids found not to be crucial for claudin-4 targeting, and to improve peptide monomer stability when synthesized in E coli (*2*), and further to result in a reduction in peptide size with the aim to produce more rapid pharmacokinetics and allow faster imaging. Additionally, a single cysteine residue was added to the sequence to allow site-specific conjugation of the peptide

to a maleimide-DTPA chelator. Amplification of the truncated cCPE from the pETH10PER plasmid (*1*), using standard PCR methodology, was performed and the clone was validated by nucleotide sequencing (Source Bioscience, Oxford UK). Oligonucleotide primers were designed in-house and synthesized by Invitrogen. Twenty-five cycles of PCR amplification was performed using the reagents and protocols of the AccuPrime Taq DNA Polymerase System (# 12339-016, Invitrogen Thermo Fisher Scientific Waltham USA). Nhe1/Nde1 restriction digest of the PCR amplicon facilitated ligation, using T4 DNA ligase (New England Biolabs, Ipswich USA), into the original pETH10PER/pET16b vector. The ligated plasmid was transformed and propagated initially into Stbl-2 cells (Invitrogen).

From this 194-319 plasmid clone a number of variants were created using QuikChange II Site-Directed Mutagenesis (SDM) (kit #200523, Agilent Technologies Santa Clara USA), or Gene Synthesis (GenScript, Piscataway USA). The SDM process was performed using the manufacturer's reagents and protocols. In brief, two oligonucleotide primers, both containing the desired mutation and complementary to opposite strands of the vector, were synthesized for each mutation required. PfuUltra HF DNA polymerase was used to extend the entire plasmid vector template. Treatment with Dpn I endonuclease digested the original parental DNA template, and the remaining nicked vector DNA containing the desired mutations was then transformed into XL1-Blue supercompetent cells. The mutated cCPE was then validated by nucleotide sequencing.

Clones S313A and S307A+N309A+S313A were created separately by SDM and Gene Synthesis, respectively – and were based on a previous report (*3*) in which peptide substitution experiments identified a number of forms exhibiting enhance affinity for

claudin-4 in a LDH release assay: S313A exhibited the greatest single point mutation effect, and S307A+N309A+S313A were a combination of the greatest effects.

Clones L254F+K257D and D284A were separately generated by SDM, and were designed in-house with a view to improving cCPE specificity for claudin-4 over claudin-3. The mutated cCPE clones were all validated by nucleotide sequencing.

Supplemental Figures

Supplemental Figure 1:

A

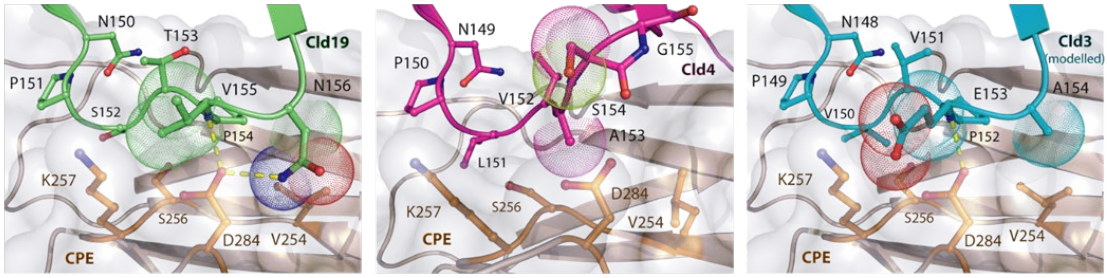

B

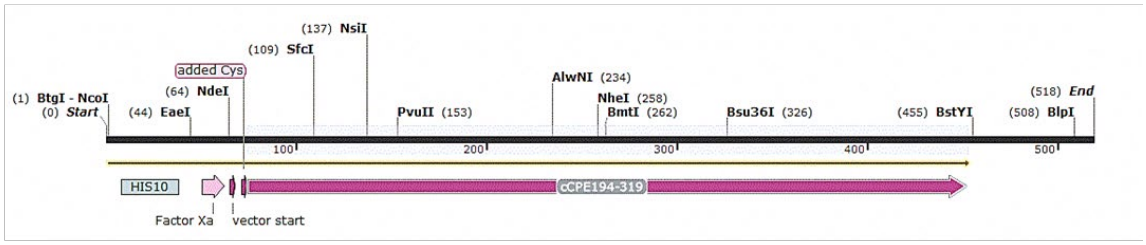

C

cCPE peptide	Sequence
$cCPE_{194-319}$	$(H_{10})cCPE_{194-249}$-KYRILASKIV DFNIYSNNFN NLVKLEQSLG DGVKDHYVDI SLDAGQYVLV MKANSSYSGNYPYSILFQKF
S313A	$(H_{10})cCPE_{194-249}$-KYRILASKIV DFNIYSNNFN NLVKLEQSLG DGVKDHYVDI SLDAGQYVLV MKANSSYSGNYPY**A**ILFQKF
S307A+N309A+S313A	$(H_{10})cCPE_{194-249}$-KYRILASKIV DFNIYSNNFN NLVKLEQSLG DGVKDHYVDI SLDAGQYVLV MKANSSY**A**G**A**YPY**A**ILFQKF
D284A	$(H_{10})cCPE_{194-249}$-KYRILASKIV DFNIYSNNFN NLVKLEQSLG DGVK**A**HYVDI SLDAGQYVLV MKANSSYSGNYPYSILFQKF
L254F+K257D	$(H_{10})cCPE_{194-249}$-KYRI**F**AS**D**IV DFNIYSNNFN NLVKLEQSLG DGVKDHYVDI SLDAGQYVLV MKANSSYSGNYPYSILFQKF

***Supplemental Figure 1*:** A) Modelling the interaction of claudin-19 (left), claudin-4 (middle) and claudin-3 (right) with wild type cCPE. B) Design of expression vector for cCPE peptides. C) cCPE mutant sequences [$(H_{10})cCPE_{194-249}$= MGHHHHHHHHHHSSGHIEGRHMLCDIEKEILDLAAATERLNLTDALNSNPAGNLYDWRSSNSYPWTQKLNLH LTITATGQ].

Supplemental Figure 2

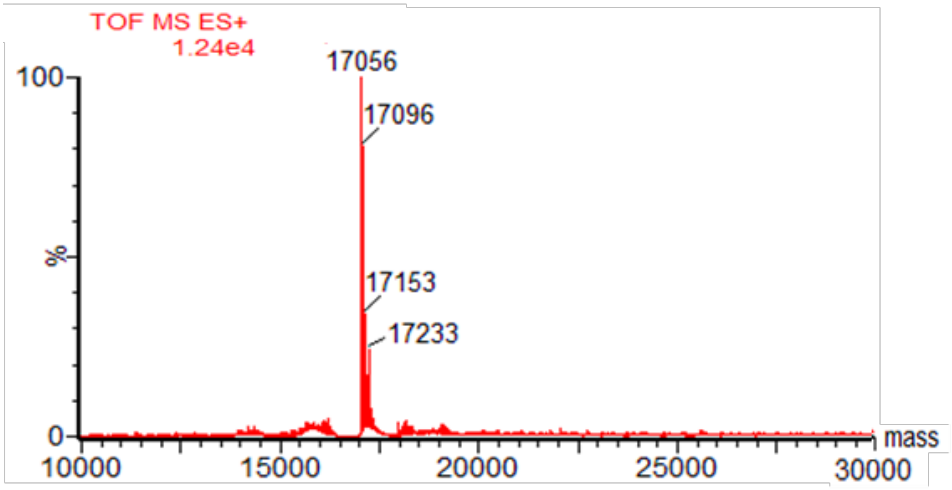

***Supplemental Figure 2*:** Mass spectroscopy of cCPE^{S313A}.

Supplemental Figure 3

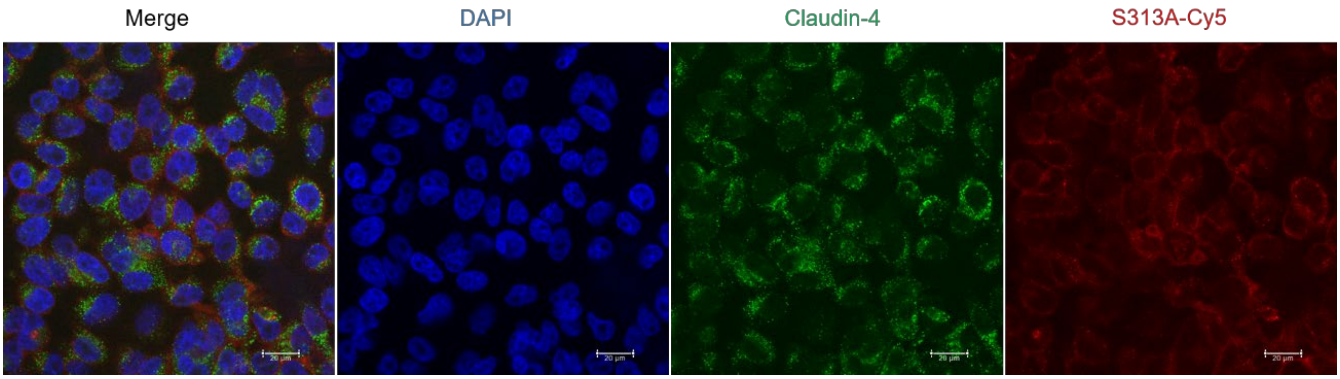

***Supplemental Figure 3*:** Confocal fluorescence microscopy images of PSN-1 cells stained with claudin-4 after incubation with S313A-Cy5 (100 nM, 30 min). Blue=DAPI; green=claudin-4; red=S313A-Cy5. Scale bar indicates 20 μm.

Supplemental Figure 4

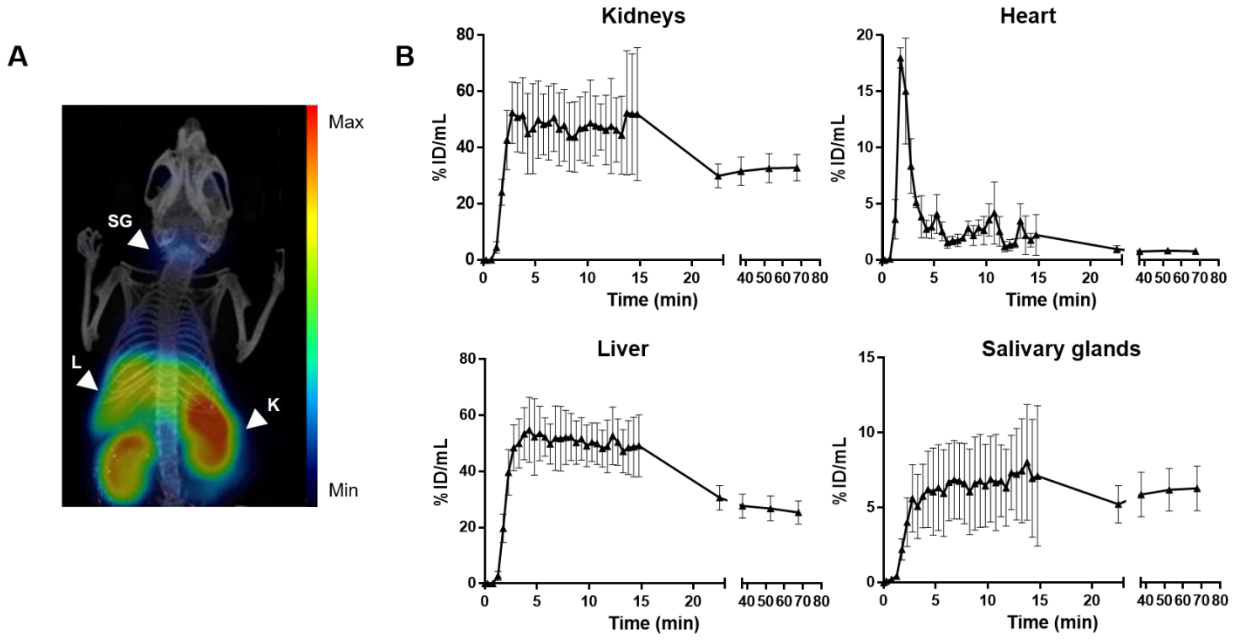

***Supplemental Figure 4*:** A) Maximum intensity projection SPECT/CT image of wildtype mouse injected with ^{111}In-DTPA-cCPE$_{194-319}$ at 90 min post-injection of the tracer. SG= salivary glands; L= liver; K= kidneys. B) Time course of ^{111}In-DTPA-cCPE$_{194-319}$ accumulation over 90 min from time of injection in kidneys, heart, liver and salivary glands in wildtype mice (n=3).

Supplemental Figure 4

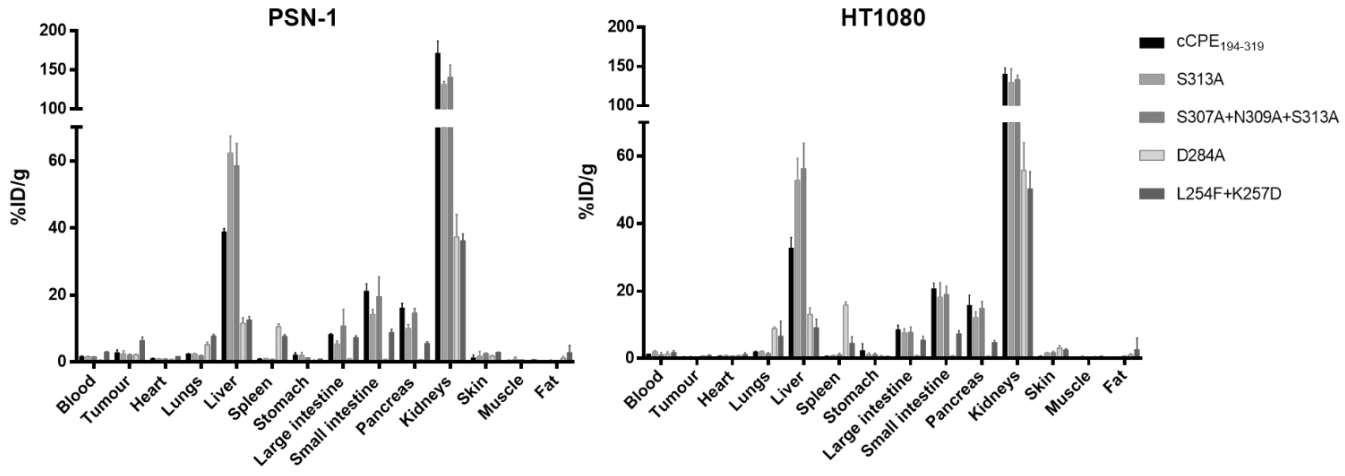

Supplemental Figure 4: Full *ex vivo* biodistribution of all ^{111}In-labelled cCPE peptides in mice bearing PSN-1 or HT1080 tumour xenografts.

References for supplemental information

1. Katahira J, Sugiyama H, Inoue N, Horiguchi Y, Matsuda M, Sugimoto N. Clostridium perfringens enterotoxin utilizes two structurally related membrane proteins as functional receptors in vivo. *J Biol Chem.* 1997;272:26652-26658.

2. Van Itallie CM, Betts L, Smedley JG, 3rd, McClane BA, Anderson JM. Structure of the claudin-binding domain of Clostridium perfringens enterotoxin. *J Biol Chem.* 2008;283:268-274.

3. Takahashi A, Komiya E, Kakutani H, et al. Domain mapping of a claudin-4 modulator, the C-terminal region of C-terminal fragment of Clostridium perfringens enterotoxin, by site-directed mutagenesis. *Biochem Pharmacol.* 2008;75:1639-1648.